Quantum spin liquid: The Heisenberg antiferromagnet on the three-dimensional pyrochlore lattice

Benjamin Canals
Laboratoire de Magnétisme Louis Néel, CNRS, Boîte Postale 166, 38042 Grenoble Cedex 9, France
and Max-Planck-Institut für Physik komplexer Systeme, Nöthnitzer Straße 38, D-01187 Dresden, Germany

Claudine Lacroix
Laboratoire de Magnétisme Louis Néel, CNRS, Boîte Postale 166, 38042 Grenoble Cedex 9, France
(Received 16 February 1999; revised manuscript received 20 July 1999)

We calculate the correlation functions of the $S=\frac{1}{2}$ Heisenberg antiferromagnet on the three-dimensional pyrochlore lattice. We use a perturbative expansion in terms of spin blocks. This method is self-controlled by the extracted correlation length. We find that the ground state is a spin-liquid state: the spin-spin correlation functions decay exponentially with distance and the correlation length never exceeds the interatomic distance, even at $T=0$. The static structure factor becomes dispersive, indicating a selection of modes by thermal and quantum fluctuations. We also calculate the magnetic neutron diffraction cross section in two planes of the reciprocal space and we find a very good agreement with neutron experiments performed on $Y(Sc)Mn_2$ and $CsNiCrF_6$.

I. INTRODUCTION

The ground state of the quantum Heisenberg antiferromagnet depends strongly on the geometry of the lattice. For simple lattices the results are well known: in one-dimensional (1D) systems quantum fluctuations destroy long-range order and make a discrepancy between integer and half-integer spin;[1] on the 2D square lattice, there is a critical point for all S at $T=0$; for the 3D cubic lattice one expects a positive T_c, for all spins. In contrast with these results, there exists a class of lattices where geometrical constraints prevent any ordering even at $T=0$; this is the case for the 2D *kagomé* lattice and the 3D pyrochlore lattice.[2] These systems, known as fully frustrated lattices have in common the triangular cell as an elementary object of the structure. Thus at least one interaction cannot be satisfied and the degeneracy of the low-energy configurations is very high.[3]

Since Anderson proposed the resonant valence bond wave function for the triangular lattice,[4] a lot of attention has been focused on frustrated structures, one of the main interest being the search for spin-liquid-like ground states in high dimensions, i.e., an absence of any critical point on lattices in two and three dimensions. First motivated by such considerations, it appeared later that many systems or compounds exhibit such unusual structures and their magnetic properties are often nonconventional, involving noncollinear or incommensurate orderings[5] or apparently broken ergodicity without structural disorder.[6–12] Thus the study of the Heisenberg model on frustrated lattices has two main interests: (i) to elaborate models where the universality class differs qualitatively from what is found on square or cubic ($D=2$, $D=3$) lattices; (ii) to understand the unconventional behavior of several experimental systems.

In this paper, we will focus on these two aspects, restricting ourselves to the pyrochlore lattice. This structure is a three-dimensional arrangement of corner sharing tetrahedra (Fig. 1). According to the Lacorre definition of frustration[13] it is probably the most frustrated structure known in compounds. Experimentally, several families of compounds are known to crystallize with this geometry. The first one is an oxide family with the general formula $A_2^{3+}B_2^{4+}O_7$ (Refs. 14–17) (A is a rare earth and B is a transition metal). The second one concerns spinels of general formula AB_2O_4 or $A_2B_2O_4$ (Refs. 17–19) (A is a rare earth and B is a transition metal). The third one concerns fluorides of general formula $AB^{2+}C^{3+}F_6$ (Refs. 20, 21) (A is an alkali metal, B and C are transition metals). The last one is the intermetallic Laves phase compounds of general formula AB_2 (Refs. 22, 23) (A is a rare earth, B is a transition metal). Strictly speaking, the only candidate that can be rigorously described by a localized, uniform Heisenberg model is the first family, as this system is well ordered with a uniform distribution of magnetically localized ions. The second and third sets often possess positional or chemical disorder[17,20] that should be taken into account in the model and the last one is better described within an itinerant model.[24] Among these compounds, a few

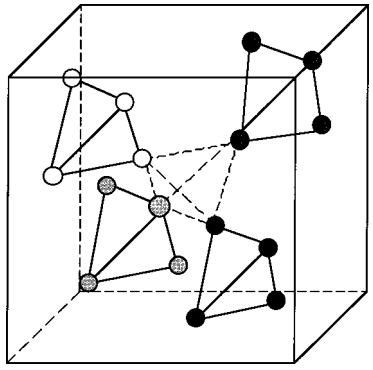

FIG. 1. Structure of the pyrochlore lattice. Plain lines correspond to J interactions, whereas dashed lines are J' interactions.

order at a well-defined Néel temperature like FeF_3,[5] $Nd_2Mo_2O_7$, or $Mn_2Sb_2O_7$,[15] while all the others have unconventional magnetic properties. In this last set, it has been experimentally observed that many common features characterize their behavior, justifying the use of localized spin models. These features may be summarized as follows: there is no magnetic ordering at any temperature or there is a spin-glass-like transition; the associated freezing temperature is of one or two orders of magnitude less than the coupling constants. As the glassy behavior is expected to derive from the highly degenerate ground state in absence of structural disorder, most studies focused on the understanding of the Heisenberg antiferromagnet on the pyrochlore structure.

The problem of ordering in the pyrochlore lattice was initiated by Anderson[25] who predicted that only long-range interactions are able to stabilize a Néel-like ground state for the Ising antiferromagnet on the pyrochlore lattice. More recently, mean-field studies for Heisenberg spins[26] have confirmed these predictions. As this system displays a classical ground state with macroscopic degeneracy, Villain[27] argued that it should behave as a *cooperative paramagnet*, with only short-range correlations down to low temperature. Classical Monte Carlo simulations on Ising and Heisenberg spins[12,28,29] confirmed that this system does not order down to zero temperature. However, any additional interaction, even very small, [easy plane anisotropy (*XY* spins), deformations, second neighbor exchange, etc . . .] will remove the degeneracy and induce magnetic ordering.[30]

Thus, the Heisenberg antiferromagnetic model with nearest-neighbors interactions is now strongly believed to have no magnetic transition, even at $T=0$. In this sense, it is a strong deviation from the behavior of the classical Heisenberg model on the 3D cubic lattice. Using spin-wave calculation, Sobral *et al.*[31] have shown that collinear fluctuations are favored. In the pure quantum case $S=\frac{1}{2}$, very little work has been done. The first attempt was performed by Harris *et al.*[32] who showed that in the $S=\frac{1}{2}$ case, the quantum fluctuations play a crucial role. Isoda *et al.*[33] used a valence bond solid approach and concluded that this system is well described by a superposition of four-sites singlets on tetrahedra. Recently, also for $S=\frac{1}{2}$, we have shown using a density-matrix perturbation expansion, that the system is never critical and the Heisenberg antiferromagnet takes into account a large part of the physics of all compounds with the pyrochlore structure.[34] Here, we will give an extended version of this work, detailing in Sec. II the model, and our method, in Sec. III the analytical results, in Sec. IV a comparison with experimental results, and we will conclude in Sec. V.

II. MODEL AND METHOD

The Hamiltonian of the quantum Heisenberg model on the pyrochlore lattice is

$$H=-J\sum_{\langle i,j\rangle} S_i\cdot S_j, \tag{1}$$

where the summation is taken over the nearest neighbors sites. J is the negative exchange coupling. The pyrochlore structure is a non-Bravais lattice but it can be described by a face centered cubic lattice (fcc) with a tetrahedral unit cell, i.e.,

$$H=-J\sum_{\langle i,j\rangle}\sum_{n,m} S_i^n\cdot S_j^m, \tag{2}$$

where (i,j) belong to the fcc lattice and $(n,m)\in\{1,2,3,4\}^2$ describe the four sites of the tetrahedral unit cell. Thus, the Hamiltonian may be decomposed into two terms; the first one corresponds to the interactions within each unit cell and the second one to interactions between these cells (Fig. 1),

$$H=-J\sum_{(i,j)\in \text{unit cell}} S_i\cdot S_j - J\sum_{\substack{(i,j)\ \text{between}\\ \text{unit cell}}} S_i\cdot S_j. \tag{3}$$

We now choose to set the interaction between different tetrahedra equal to J', in order to make a formal expansion with respect to the parameter $\lambda=J'/J$. Of course the starting model [Eq. (2)] corresponds to $\lambda=1$.

$$H=-J\sum_{(i,j)\in \text{unit cell}} S_i\cdot S_j - J'\sum_{\substack{(i,j)\ \text{between}\\ \text{unit cell}}} S_i\cdot S_j. \tag{4}$$

In order to perform this expansion, we first diagonalize exactly each tetrahedron corresponding to a unit cell. The number of eigenstates for this unit cell is 16 (four spins $\frac{1}{2}$): these 16 levels split into a two-fold degenerate singlet (ground state) with energy $3J/2$ and excited states of energy $J/2$ (degeneracy$=9$) and $-3J/2$ (degeneracy$=5$). The corresponding 16 eigenstates are calculated analytically and form a diagonal base for this small system (Appendix A). We then consider the second part of the Hamiltonian, which couples all the sets of 16 levels together. At this stage, we have made a correspondence between the Heisenberg Hamiltonian on the pyrochlore lattice and a quantum system formed by an fcc lattice where each site has 16 available states. If $J'=J$ the correspondence is exact but unfortunately it cannot be solved. Our assumption is to consider that $\lambda=J'/J$ is small and to make an expansion in powers of λ. At the end of the calculation, we put $\lambda=1$ again to recover the initial Heisenberg Hamiltonian. The validity of this approximation is driven by the correlations that develop in the system: it is straightforward to see that for an ordered magnetic system, this approximation will give an unreasonable conclusion as the correlation length will diverge; an infinite correlation length requires the expansion to be made to all orders in λ. But within a magnetically disordered ground state, with a small correlation length, this method should provide (indeed it does) a good approximation as it exactly sums a large number of spin configurations. Furthermore, there is no boundary effects like in exact diagonalization approaches as none of the symmetries are broken here. Thus, as soon as the calculations are self justified (depending on the final correlation length deduced), this method gives accurate results within a wide temperature range.

All the thermodynamical quantities can be obtained from the density operator, which we calculate in perturbation with respect to $\lambda=J'/J$

$$\rho=e^{-\beta H}=\rho_0+\cdots+\rho_n+\Theta(\lambda^n), \tag{5}$$

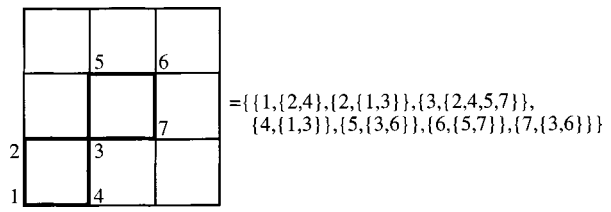

FIG. 2. Example of a graph in the *bipartite* square lattice. The list is built with the number of each site and its corresponding neighbors.

where ρ_n is of order λ^n:

$$\rho_n=(-1)^n\int_0^\beta\int_0^{\beta_1}\cdots\int_0^{\beta_{n-1}}d\beta_1\cdots d\beta_n \times e^{-(\beta-\beta_1)H_0}H_1\cdots e^{-(\beta_{n-1}-\beta_n)H_0}H_1e^{-\beta_nH_0}. \quad (6)$$

In order to evaluate the different terms of the development, we have made an analogy between these calculations and the usual high-temperature (HT) expansions. In such expansions, one has to define an equivalence relation on the set of graphs built on the underlying lattice. The way we did the classification of the graphs is the following: for a given graph, we number the sites $\{1,...,n\}$; we associate to each of these sites its nearest neighbors. We finally obtain a list, illustrated in Fig. 2 by a graph on the square lattice.

For another graph, we also built its characteristic list. If we are able to find a permutation that identifies the second list to the first one, then the graphs will belong to the same class. This is the main idea of this equivalence relation. In fact, we have to add other indices because we have introduced a formal anisotropy when we do a differentiation between the four types of sites (1, 2, 3, or 4) in the nonbipartite pyrochlore lattice. We also give an illustration for the square lattice on Fig. 3, where we have considered a graph built within a four-sites unit-cell lattice.

These indices are not affected by the permutation as they reflect an arbitrary choice for the calculation. Given the classes corresponding to a particular order in λ, we evaluate all graphs analytically by implementing all the calculations on a workstation in a MATHEMATICA code.[35] The advantage is that we obtain analytical results, i.e., functions depending analytically on the parameters β, J, and J'.

The main difference between this method and a standard HT development is the absence of divergence at zero temperature. While in usual HT, one has to use low-temperature approximations of the HT results (Padé approximants for

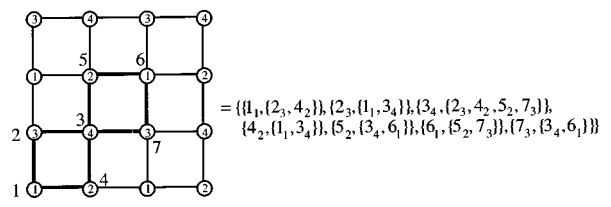

FIG. 3. Illustration of a list when the unit cell is a group of four sites (as it is the case in the pyrochlore lattice). The number of sites are no longer sufficient (big numbers) to identify a link; we need to consider the type of each site (small numbers in circles) to know the nature of a bond.

example), here each order in λ sums an infinite number of terms and this guarantees the convergence of the series at all temperatures.

III. RESULTS: SPIN-SPIN CORRELATION FUNCTIONS AND STATIC STRUCTURE FACTOR

Let us consider a reference site S_0 on the lattice. We define $\langle \mathbf{S}_0\cdot\mathbf{S}_d\rangle = C_d$ as the correlation function between this site and a site at a distance d in the lattice. This function is easily evaluated as

$$C_d=\frac{1}{Z}\mathrm{Sp}[\mathbf{S}_0\cdot\mathbf{S}_d\rho], \quad (7)$$

where Z is the partition function. The development was made up to second order in λ, which allows us to calculate C_d up to the sixteenth neighbors. Making a development in λ^2 in C_d is equivalent to making a development in λ^3 for Z. Explicitly, one has to compute ρ to third order as

$$\rho=\rho_0+\rho_1+\rho_2+\rho_3, \quad (8)$$

where ρ_n is given by Eq. (6), and

$$Z=\mathrm{Sp}(\rho)=Z_0+Z_1+Z_2+Z_3, \text{ where } Z_n=\mathrm{Sp}(\rho_n). \quad (9)$$

The initial base for the computation of the spur is the tensorial product of all the diagonal eigenstates of N exactly diagonalized tetrahedra, i.e.,

$$|1_0\rangle=\prod_i^{\otimes}|1_0^i\rangle, \quad (10)$$

where $|1_0^i\rangle$ is one of the 16 eigenstates of the ith tetrahedron. The way we did the computations and the geometrical algorithm we build are described in Appendix B. But one can see immediately that each order n in λ involves the same number n of bounds of the fcc lattice, and each H_1 operator acts on a base constituted by the product of two eigenstates of neighboring tetrahedron. Thus, each order n involves the evaluation of $(16\times16)^n$ terms. This means that the third order involves $(16\times16)^3=16\ 777\ 216$ terms and this is multiplied by the number of geometrical diagrams one can find in an fcc lattice. Moreover, in λ^3 calculations, each term is formed with a triple integral. Of course, the main difficulty is to calculate all the terms of the series. For example, the evaluation of the spin-spin correlation functions from the first to the sixteenth neighbors took approximately one month and a half of CPU time. This is in fact the limiting factor in our approach.

Using our method, we evaluate the spin-spin correlation functions for $d=0$ (auto correlation), $d=1$ (nearest-neighbors correlations), . . ., $d=5$ (sixteenth neighbors correlations). We have reported in Fig. 4 the geometry of the lattice, including only the sites up to the seventh neighbors for clarity. We observe that for some distances, there exists different topologies, therefore we introduce a numbering that includes this particular point, for example 3_1 and 3_2 for which $d=1$ (see Fig. 4).

To look for the possibility of a critical point, we have studied the variation of these correlation functions with temperature. First, their signs remain constant, i.e., for one given

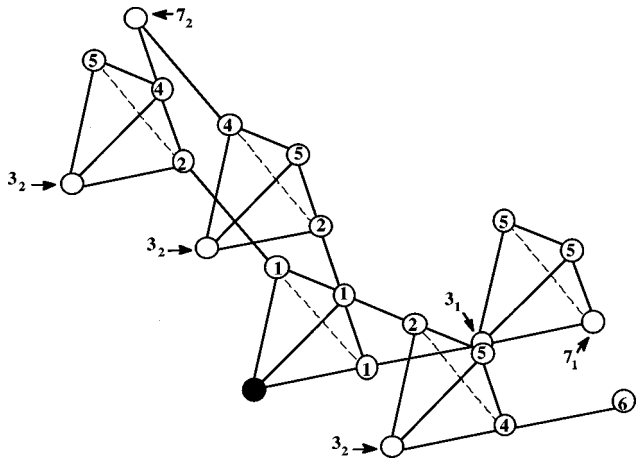

FIG. 4. Geometry of the lattice up to the seventh neighbors. The black point is the ''origin'' site. The numbers in the white points indicate the nth neighbors. The indices differenciate the types of neighbors as explained in the text.

distance, the amplitude is varying with the temperature but the sign of the correlation is constant over all the temperature range. The corresponding distances and signs are reported in Table I.

As none of these correlation functions exhibit a critical behavior, we have studied the behavior of these functions with the separation distance in the lattice. As shown in Fig. 5, whatever the temperature, the correlations decay exponentially with the separation distance. This characteristic was already observed in the *kagomé* lattice.[36] One can see that for a given distance, there might be several points. This is not due to numerical uncertainties but to the geometry of the lattice that allows different topologies for a given distance. For each temperature, we extract a correlation length defined as $C_d \propto e^{-d/\xi}$. This length is temperature dependent and never exceeds one interatomic distance down to zero temperature (see Fig. 2 in Ref. 34); the broad feature at $T \approx J$ shows, as expected, that this method is less controlled when $T < J$. Assuming that ξ could be underevaluated for $T \leqslant J$ by our method, we extrapolated $\xi(T)$ from the $T \geqslant J$ regime to the low-T regime. Whatever the law we used (algebraic, exponential, stretched exponential), we found a saturation of the correlation length around the interatomic distance. Thus, our calculations are self-consistently controled as the value of ξ at $T=0$ is much smaller than the real spatial extension of our development (five interatomic distances).

The total spin can be obtained from the spin-spin correlation function as

$$\left\langle \left(\sum_{i=1}^{N} \mathbf{S}_i \right)^2 \right\rangle = NS(S+1) + 6NC_1 + 12NC_2 + \cdots , \tag{11}$$

where N is the number of sites and C_1 and C_2 the nearest- and next-nearest-neighbors correlation functions. Since we have shown that these correlation functions are rapidly decreasing with distance, we can retain only a few terms in this expansion. Cutting the summation to the second neighbors, we verify that the ground state is a singlet:[37]

$$\frac{1}{N} \left\langle \left(\sum_{i=1}^{N} \mathbf{S}_i \right)^2 \right\rangle (T=0) \cong -0.02. \tag{12}$$

This negative value is of course an artifact but one has to take into account that we cut the sum to the second order (with $C_1 \approx -0.186$ and $C_2 \approx 0.029$ at $T=0$). In fact, this sum is an alternated one as the sign of the correlations is oscillating with distance (see Table I). Furthermore, this method is not supposed to be accurate in this temperature range. Surprisingly, it is even satisfactory at low temperature as the obtained total spin value is negligible compared to $S(S+1)$. This is essentially because the correlations inside each unit cell are calculated exactly, and in a quantum spin liquid, only short-range correlations are important.

Nevertheless, this calculated C_1 is certainly overestimated. Comparing with Harris *et al.*[32] (who found a ground-state energy, $E \approx -0.49|J|$) and Isoda *et al.*[33] (who found $E \approx -0.46|J|$), our C_1 gives $E \approx -0.56|J|$. These three values are obtained through different types of expansions in J'/J, and should be compared with other methods: for ex-

TABLE I. Signs of spin-spin correlations as a function of intersite distance in the lattice. The corresponding number of steps is also reported.

Neighbor	Intersite distance and number of steps in the lattice	Sign of correlations	Neighbor	Intersite distance and number of steps in the lattice	Sign of correlations
1	1, 1	−	9_3	$2\sqrt{3}$,4	+
2	$\sqrt{3}$,2	+	10_1	$\sqrt{13}$,4	+
3_1	2, 2	+	10_2	$\sqrt{13}$,4	−
3_2	2, 3	−	11	$\sqrt{15}$,5	−
4	$\sqrt{5}$,3	−	12_1	4, 4	+
5	$\sqrt{7}$,3	−	12_2	4, 5	−
6	$2\sqrt{2}$,4	+	13_1	$\sqrt{17}$,5	−
7_1	3, 3	−	13_2	$\sqrt{17}$,5	−
7_2	3, 4	+	14	$\sqrt{19}$,5	−
8	$\sqrt{11}$,4	+	15	$\sqrt{21}$,5	−
9_1	$2\sqrt{3}$,5	−	16	5, 5	−
9_2	$2\sqrt{3}$,5	+			

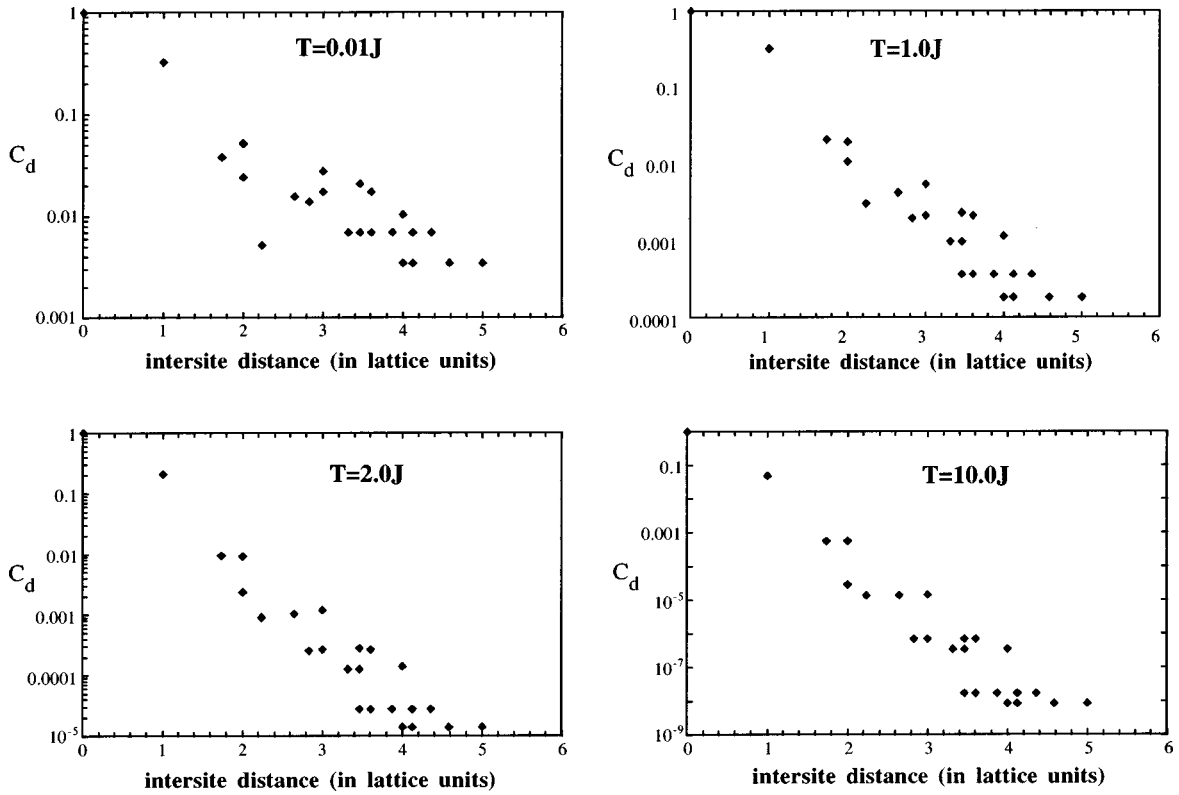

FIG. 5. Evolution of the spin-spin correlation $C_d = |\langle \mathbf{S}_0 . \mathbf{S}_d \rangle|$ with the intersite distance at different temperatures.

ample, preliminary results using exact diagonalization for a 16-site cluster[38] give $E \approx -0.55|J|$, but it would be necessary to study larger clusters.

We also point out that the control of the calculations via the calculated correlation length does not exclude other types of ordering within this model. Order parameters involving three or four spins like dimer-dimer, spin Peierls, or chiral, cannot be tested with our method (see, for example, Ref. 32).

With the correlation functions calculated above, we can evaluate the static structure factor. Usually, in magnetic systems the maximum of the structure factor indicates which magnetic structure is stabilized at the mean-field Néel temperature. For classical spins treated in a mean-field approximation (MFA) in the pyrochlore lattice, this quantity is very peculiar: it possesses two branches of zero-energy modes, completely flat over the entire Brillouin zone, and two other dispersive branches.[26] In MFA, this means that the system can move from one state to another without energy cost, as soon as the temperature is below the mean-field critical temperature. So this temperature does not correspond to a magnetic ordering, it only means that the system acquires a local magnetization but macroscopic degeneracy is still present; thus the system remains magnetically disordered.

In order to study the effect of quantum and thermal fluctuations (not taken into account in MFA) on the flat modes, we evaluated the structure factor,

$$S^{m,n}(\mathbf{q}) = \sum_d C_d e^{i\mathbf{q}\cdot\mathbf{R}_d^{m,n}}, \tag{13}$$

where m and n are the indices of a site in a tetrahedral unit cell $[(m,n) \in \{1,2,3,4\}^2]$. C_d is defined in Eq. (7), $\mathbf{q}$ is a vector of the first Brillouin zone, and $\mathbf{R}_d^{m,n}$ is the vector of length d that links the sites of type m and n. As this lattice is not a Bravais Lattice, for each $\mathbf{q}$ this structure factor will be a 4×4 matrix, whose eigenvalues give the fluctuation modes of the system, the lowest energy mode corresponding to the largest eigenvalue $\omega_M(q)$. To first order in λ, $\omega_M(q)$ remains nondispersive over the entire Brillouin zone (BZ), and degeneracy is not lifted. To the second order, a maximum appears on the axis Δ (see Fig. 3 in Ref. 34) of the Brillouin zone. This maximum corresponds to a collinear phase where the total spin vanishes on each tetrahedron and the phase between two neighboring tetrahedra is equal to π. This type of ''order by disorder,'' [39,40] i.e., the selection of a particular mode with respect to the others, was already observed on the $S = \frac{1}{2}$ *kagomé* system and conjectured with classical spins on the pyrochlore lattice. Nevertheless, we note that the degeneracy is very weakly lifted ($1/10^6$ of the width of the spectrum). This is also a point in common with the *kagomé* system. But as in the *kagomé* case, we cannot exclude that the next order in λ will modify the dispersion curve. Despite this, the fact that the selected mode corresponds to the principal one appearing in neutron cross sections (see Sec. IV) is a good indication of the relevance of this result. Finally, we emphasise that this result is not a numerical artifact (as the tiny dispersion could suggest) since in our method, this structure factor is calculated analytically so that the precision can be as small as we want.

IV. COMPARISON WITH EXPERIMENTS: MAGNETIC NEUTRON CROSS SECTION

From the spin-spin correlation functions obtained via our method, we are able to compute the magnetic neutron cross section in the reciprocal space (Fig. 6). This neutron mag-

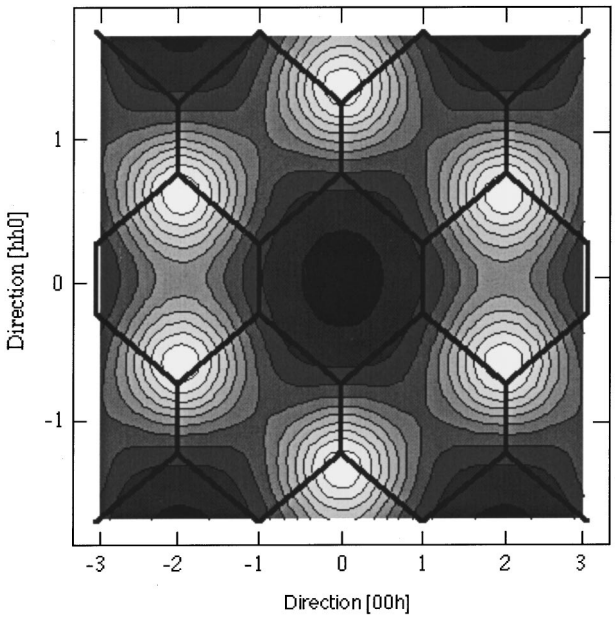

FIG. 6. Neutron magnetic cross section in the ([00h],[hh0]) plane. The superimposed structure is the trace of the extended Brillouin zone of the fcc lattice in this plane.

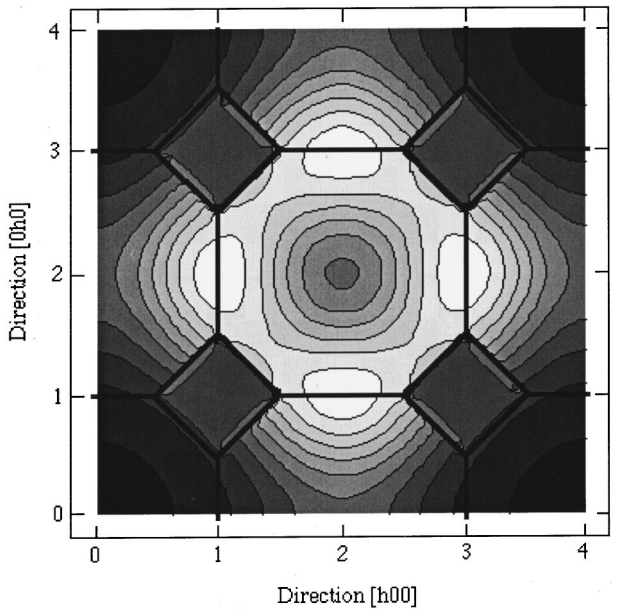

FIG. 7. Neutron magnetic cross section in the ([h00],[0h0]) plane. The superimposed structure is the trace of the extended Brillouin zone of the fcc lattice in this plane.

netic cross section is related to the spin-spin correlations by the expression

$$\frac{d^2\sigma}{d\Omega d\omega} = \sum_{m,n}^{\{1,2,3,4\}^2} e^{-i\boldsymbol{\kappa}\cdot(\mathbf{T}_m-\mathbf{T}_n)} U_{m,n}(\mathbf{Q},\omega), \qquad (14)$$

where

$$U_{m,n}(\mathbf{Q},\omega) = \sum_{i,j} e^{-i\mathbf{q}\cdot(\mathbf{R}_i-\mathbf{R}_j)} \times \sum_{m,n} e^{-i\mathbf{q}\cdot(\mathbf{T}_m-\mathbf{T}_n)} \int_{-\infty}^{+\infty} \langle \mathbf{S}_{i,m}(0)\mathbf{S}_{j,n}(t)\rangle e^{-i\omega t} dt. \qquad (15)$$

T_m and R_i are the translations which determine the position of a site of type m in the unit cell i of the space group $Fd\bar{3}m$; $Q=\kappa+q$, where κ is a vector of the reciprocal lattice and q belongs to the first BZ. From the static correlation functions calculated above, we obtain the total magnetic cross section $d\sigma/d\Omega$. We have calculated the neutron cross section in two planes of the reciprocal lattice, namely the ([00h],[hh0]) plane and the ([h00],[0h0]) plane shown, respectively, in Figs. 6 and 7. The intensity in the ([00h],[hh0]) plane is maximum around the points $Q_1=[200]\pm[\frac{3}{4}\frac{3}{4}0]$ or $Q_1'=[002]\pm[\frac{3}{4}\frac{3}{4}0]$. These maxima describe correlations that correspond to an ordered structure where consecutive tetrahedra are in phase. This is in contradiction with the results obtained from the static structure factor in the preceding section. Nevertheless, the study of the other plane provides an explanation of this phenomena: in the ([h00],[0h0]) plane, the maximum intensity is around $Q_2=[210]$, which corresponds to a phase π between consecutive tetrahedra, as expected from the static structure factor. Thus our conclusion is the following: there exist two characteristic modes in this system, a π-dephased one and an in-phase one. When comparing the intensities of these modes, we observe that the first one has the larger weight in agreement with the results of Sec. III. This compatibility of the two approaches is not straightforward as Eq. (15) shows that the four branches of the static structure factor contribute to the cross section.

It is interesting to compare our results with both experimental and previous theoretical results: experiments performed on Y(Sc)Mn_2 by Ballou *et al.*[41] and on $CsCrNiF_6$ by Harris *et al.*[20] are well reproduced by our calculations (Figs. 6 and 7); in both cases, these results were obtained for a given energy ω but the shape of the neutron cross section in reciprocal space was found to be nearly independent of the energy,[41] as if $\chi(q,\omega)=f(q)g(\omega)$. Thus, integrating the experimental results over the energy does not change the q dependence and we can make a direct comparison between our calculations (based on equal time correlations) and the measured map: (i) First we reproduce all the main features previously obtained, i.e., the absence of signal in the first BZ associated with the singlet ground state and the maxima at Q_1 and Q_1'. (ii) Second, we find a π-dephased mode in the ([h00],[0h0]) plane that was also observed in the same compound.[42] The existence of these two modes could explain the first-order character of the transition observed in the pure YMn_2 compound. When Sc is absent, this compound undergoes a structural transition at 100 ± 10 K, which is suppressed in the presence of Sc. At the transition, a Néel ordering appears, corresponding to the π-dephased phase, which was found to have the largest intensity in the calculation. We attribute this first-order transition to the freezing of this mode at the same temperature, as its weight is slightly larger than the in-phase mode. However we point out again that a phase transition can occur only if other interactions are present in the system. In this case, this could be the magnetoelastic interactions.[43] (iii) Third, the half-width of each

peak provides information on the correlation length: it is found to be around one interatomic distance in experiments as well as in our calculations.

Theoretically, we recover the results concerning classical Monte Carlo simulations[3,20] performed on the pyrochlore lattice and dealing with the magnetic fluctuations in the $([hh0],[00h])$ plane of the reciprocal lattice. We also give evidences for another type of magnetic fluctuations in the $([h00],[0h0])$ plane that was not obtained in previous classical calculations. This means that the most important features of the magnetic modes are coming from the structure, as our quantum localized model is able to explain experimental results performed on both localized and itinerant systems, and to reproduce results obtained for classical spin systems.

V. DISCUSSION

In this paper we have presented an analytical expansion for the quantum Heisenberg antiferromagnet on the pyrochlore lattice. Our results show that there is no magnetic transition in this three-dimensional system, even at $T=0$. The spin-spin correlations are exponentially decaying with distance at all temperatures and the correlation length is always finite. The static structure factor becomes dispersive but the amplitude of its dispersion is extremely small, excluding any mean-field analysis. The calculated neutron cross sections correspond to the experimental ones. We have shown that two magnetic modes coexist in this system but with different amplitudes.

All these results are very unusual as the same Hamiltonian usually exhibits a transition on regular lattices. So this behavior is not only quantitatively different but *qualitatively* different. We attribute this strong deviation from the conventional behavior to the complete frustration of the Heisenberg model on the pyrochlore lattice. This absence of order seems to be very similar to the one predicted theoretically on the two-dimensional *kagomé* lattice, at least concerning the spin-spin correlations and the static structure factor. Concerning the magnetic cross section, we notice that the fluctuations in the $([hh0],[00h])$ plane are similar to the one in the *kagomé* plane.[36,44] This is not surprising as the section along the (111) axis of the pyrochlore structure is a *kagomé* plane.

More surprising is the coincidence of the theoretical results obtained via our localized model and the measurements performed on $Y(Sc)Mn_2$ (Ref. 41) which is usually described as an itinerant system. Even the quantum nature of the spins does not seem to play an important role as the classical Monte Carlo simulations[3] provide much information close to the characteristics obtained in the quantum case (neutron structure and spin-spin correlations). Thus this indicates that the low-energy part of the physics in the pyrochlore structure-based compounds is mainly related to the geometry of the lattice and that this geometry prevents any magnetic ordering in localized as well as in itinerant systems.

This lack of ordering, or spin-liquid behavior, addresses the question of the structure of the low-lying levels in such a localized model. It is now believed that in 2D (the *kagomé* case) there is a spin gap, but the singlet excitations are built with a continuum starting from the ground state.[36] This is strikingly different from the usual 1D case (Haldane integer spins chains) where there is a gap in singlet excitations. In 3D (the pyrochlore case), this question is still open and motivates further studies by exact diagonalization.

The spin-glass behavior observed experimentally is also an exciting problem as, up to now, no dynamical calculation has been done on the quantum Heisenberg antiferromagnet on the pyrochlore lattice and Monte Carlo simulations have not reproduced a broken ergodicity within the isotropic Heisenberg antiferromagnet on this lattice.[3] In the classical case, this discrepancy with the experimental observations raises the importance of the dynamics. We must note that despite an absence of broken ergodicity, Moessner and Chalker[3] have shown that the low-energy density of states is high, which is an expected ingredient for a spin-glass-like behavior. As the experimental measurements have a threshold below which it is impossible to detect structural disorder, it may be possible to attribute this glassy behavior to the sensitivity of the low-energy part of the spectrum to a very small structural perturbation. Thus, such an unconventional modification of the dynamics should be studied with the appropriate tools of spin-glass theory and no longer within the frame of the isotropic Heisenberg model (quantum or classical).

These two points, dynamics and low-energy physics, are probably the more promising investigations for the near future in order to find a more accurate description and understanding of this family of compounds.

APPENDIX A: EIGENVALUES AND EIGENVECTORS OF THE UNIT CELL: EXACT DIAGONALIZATION OF ONE TETRAHEDRON

We show below the structure of the eigenstates as linear combinations of initial 4-spin up-down states.

$$|1\rangle=\frac{1}{2}(-|+-+-\rangle+|-++-\rangle+|+--+\rangle -|-+-+\rangle),$$

$$|2\rangle=\frac{2}{\sqrt{12}}(|++--\rangle-|+-+-\rangle-|-++-\rangle -|+--+\rangle-|-+-+\rangle+|--++\rangle),$$

$$|3\rangle=\frac{1}{\sqrt{2}}(-|+++-\rangle+|++-+\rangle),$$

$$|4\rangle=\frac{1}{\sqrt{6}}(-|+++-\rangle-|++-+\rangle+2|+-++\rangle),$$

$$|5\rangle=\frac{1}{\sqrt{12}}(-|+++-\rangle-|++-+\rangle-|+-++\rangle +3|-+++\rangle),$$

$$|6\rangle=\frac{1}{\sqrt{2}}(-|-++-\rangle+|+--+\rangle),$$

$$|7\rangle=\frac{1}{\sqrt{2}}(-|++--\rangle+|--++\rangle),$$

$$|8\rangle=\frac{1}{\sqrt{2}}(-|+-+-\rangle+|-+-+\rangle),$$

$$|9\rangle=\frac{1}{\sqrt{2}}(-|---+\rangle+|--+-\rangle),$$

$$|10\rangle=\frac{1}{\sqrt{6}}(-|---+\rangle-|--+-\rangle+2|-+--\rangle),$$

$$|11\rangle=\frac{1}{\sqrt{12}}(-|---+\rangle-|--+-\rangle-|-+--\rangle+3|+---\rangle),$$

$$|12\rangle=|++++\rangle,$$

$$|13\rangle=\frac{1}{2}(|+++-\rangle+|++-+\rangle+|+-++\rangle+|-+++\rangle),$$

$$|14\rangle=\frac{1}{\sqrt{6}}(|++--\rangle+|+-+-\rangle+|-++-\rangle+|+--+\rangle+|-+-+\rangle+|--++\rangle),$$

$$|15\rangle=\frac{1}{2}(|---+\rangle+|--+-\rangle+|-+--\rangle+|+---\rangle),$$

$$|16=|----\rangle.$$

The local Hamiltonian may be rewritten in term of the local total spin:

$$H=-\frac{J}{2}(S^2-3)$$

with the three eigenvalues:

$$H(S=2)=-\frac{3J}{2},\quad H(S=1)=\frac{J}{2},\quad H(S=0)=\frac{3J}{2}.$$

For each value of the total spin, the subeigenspace is made of the previous eigenstates:

$$S=0:|1\rangle,|2\rangle\quad\text{(two singlets)},$$

$$S=1:|3\rangle,|4\rangle,|5\rangle,|6\rangle,|7\rangle,|8\rangle,|9\rangle,|10\rangle,|11\rangle\quad\text{(three triplets)},$$

$$S=2:|12\rangle,|13\rangle,|14\rangle,|15\rangle,|16\rangle,\quad\text{(one 5-uplet)},$$

APPENDIX B: DETAILS OF THE METHOD FOR THE COMPUTATION OF GEOMETRICAL DIAGRAMS

The method we use is a generalization of the usual high-temperature algorithm. For a given lattice, one should: (i) identify all the possible geometrical diagrams in the lattice for a given order of the development; (ii) classify these diagrams in order to avoid evaluation of equivalent diagrams; (iii) evaluate the remaining diagrams. We have first to derive the properties that allow the evaluation of any diagram without cost in time and energy. For this purpose, we derived three properties, sufficient to write all possible diagrams in a very simple way.

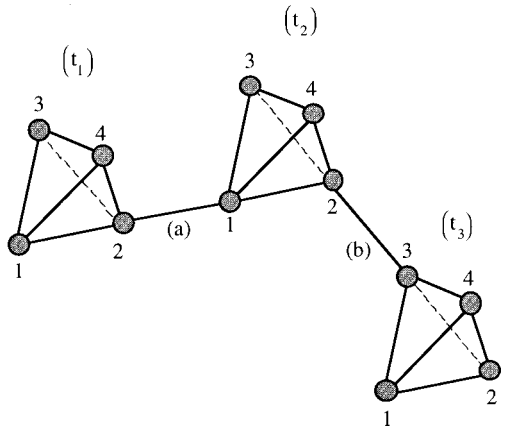

FIG. 8. Two types of connections between two nearest-neighbor tetrahedra; (a) is a 1–2 type and (b) is a 2–3 type. This formal anisotropy disappears when computing any physical quantity.

Derivation of the properties

A diagram is defined by a number of sites, linked by a number of links, one or more. For example, Figs. 8 and 9 show diagrams of the second order. In the diagram of Fig. 8, all sites of the tetrahedra are shown, whereas in Fig. 9, each point is one tetrahedron, i.e., a 16-states system. The main difference with the usual HT is that each site (point here) is not a site of the original lattice but a set of 16 states (see Appendix A), representing the physics of one tetrahedron. Thus, the rules are no longer the same and one has to properly establish these rules.

Property 1: If in a diagram one site is only one time connected, then the spur of this diagram vanishes.

Consider a diagram where one site is only once connected (Fig. 10). Let b_2 be the site that appears only once. It belongs to the bond $b=\{b_1,b_2\}$. The associated operator is $h_1^b=S_{b_1}.S_{b_2}$. In order to evaluate the spur, one has to introduce as many closure relations as there are H_1 operators in the considered term:

$$1=\sum_{|l_0'\rangle}|l_0'\rangle\langle l_0'|=\sum_{|l_0'\rangle}\left\langle\prod_u^{\otimes}\left|l_0'^u\right\rangle\right\rangle\left\langle\prod_v^{\otimes}\left|l_0'^v\right\rangle\right\rangle. \qquad \text{(B1)}$$

As b_2 appears only once in the expression, one can isolate the integrand

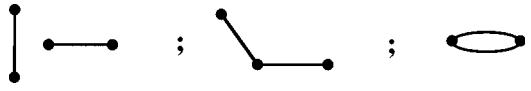

FIG. 9. Three diagrams of order λ^2. Each ''site'' represents 16 states, i.e., one tetrahedron.

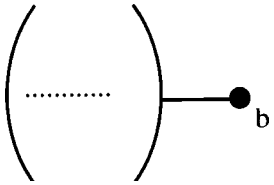

FIG. 10. General diagram with an isolated site b_2. This site represents 16 states, i.e., one tetrahedron. The dashed line represents any geometrical diagram connected to the b_2 site.

$$e^{-(\beta_n-\beta_{n+1})}[E(l_0''^{b_1})+E(l_0^{b_2})]\langle l_0''^{b_1}|\langle l_0^{b_2}|\mathbf{S}_{b_1}.\mathbf{S}_{b_2}|l_0'^{b_1}\rangle|l_0^{b_2}\rangle \tag{B2}$$

from the complete expression involving all operators and integrations. Here, $E(l_0^u)$ is the eigenvalue corresponding to the energy of the l_0^u state, i.e., one of the nonperturbed states of the uth tetrahedron. This expression is the only term where the b_2 site appears. In the computation of the spur, one can make the summation over this site, and also restrict this sum to each eigenspace where $E(l_0^{b_2})$ is constant. In this way, one has just to compute $\langle l_0^{b_2}|S_{b_2}|l_0^{b_2}\rangle$ without any prefactor, and this is equal to zero due to the spin conservation; this is the required result.

Property 2: In the complete sum corresponding to the spur, the number of distinct states on a single site is equal to the number of connections reaching this site in the corresponding diagram.

Let us consider a diagram where the site b_2 is twice connected (Fig. 11). The first step is to insert all the closure relations. Then, one gets a term of the type

$$\langle l_0'''^{b_1}|\langle l_0'''^{b_2}|\mathbf{S}_{b_1}.\mathbf{S}_{b_2}|l_0'''^{b_1}\rangle|l_0'''^{b_2}\rangle\cdots \times\langle l_0''^{b_1}|\langle l_0''^{b_2}|\mathbf{S}_{b_1}.\mathbf{S}_{b_2}|l_0'^{b_1}\rangle|l_0'^{b_2}\rangle. \tag{B3}$$

In the total expression, this is the only operator where b_2 appears. All the other terms are diagonal for this site as they are constituted by H_0-based operators or H_1-based operators, without b_2. But all the states not separated by an operator independent of b_2 have to be equal; this means that

$$|l_0'''^{b_2}\rangle=|l_0^{b_2}\rangle;|l_0'''^{b_2}\rangle=|l_0''^{b_2}\rangle;|l_0'^{b_2}\rangle=|l_0^{b_2}\rangle. \tag{B4}$$

Finally, the term where the b_2 site appears will be

$$\langle l_0'''^{b_1}|\langle l_0'''^{b_2}|\mathbf{S}_{b_1}.\mathbf{S}_{b_2}|l_0'''^{b_1}\rangle|l_0''^{b_2}\rangle\cdots \times(l_0''^{b_1}|\langle l_0''^{b_2}|\mathbf{S}_{b_1}.\mathbf{S}_{b_2}|l_0'^{b_1}\rangle|l_0^{b_2}\rangle, \tag{B5}$$

and it contains two distinct types of states $|l_0^{b_2}\rangle$ and $|l_0''^{b_2}\rangle$. For a n-connected site, the demonstration is exactly the same, so we have the desired results.

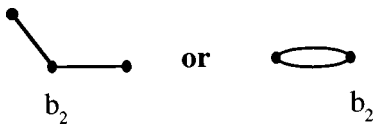

FIG. 11. Two diagrams of order λ^2. In both cases, the site b_2 is twice connected and will generate two distinct types of states, $|l_0^{b_2}\rangle$ and $|l_0''^{b_2}\rangle$ as explained in the text.

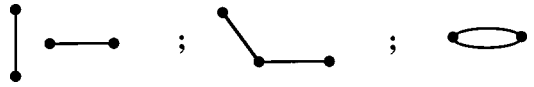

FIG. 12. Three representatives of all possible topologically equivalent diagrams of order λ^2. Only the last one gives a contribution.

As a corollary of this property, we can show that the exponential prefactor is also simplified. We have to write not only the operators but the total integrand of each term. Thus, the prefactor will be the exponential factor with the energy of each state.

Property 3: If M is the number of sites in a diagram and N the number of sites in the effective lattice, then the final expression will have z_0^{N-M} as prefactor, where z_0 is the partition function of one tetrahedron.

This result is easy to obtain. We remark that the only effective operators on the nonperturbed states are the H_1 operators. For a given diagram, these H_1 act only on the M sites. Then, the remaining N-M sites are modified only by the $e^{-(\beta_n-\beta_{n+1})H_0}$ operators, which are diagonal in this basis. For each state $k\in\{1,2,...,N-1,N\}\backslash\{M \text{ sites}\}$ we obtain the product

$$e^{-(\beta-\beta_1)E(l_0^k)}e^{-(\beta_1-\beta_2)E(l_0^k)}\cdots e^{-\beta_nE(l_0^k)}=e^{-\beta E(l_0^k)}. \tag{B6}$$

And after the summation over all $|l_0^k\rangle$, this term will give z_0. As it appears N-M times, we will finally obtain z_0^{N-M}, this is the required result.

This set of properties allows a very quick way to make calculations. Coming back to the second order, one has to evaluate three kinds of diagrams shown in Fig. 12: the first property indicates that only the third diagram does not vanish. This diagram involves two sites, this is the number of distinct states that will appear in the spur. The prefactors are given by the corollary of property 2. We now write these rules in a geometrical way (Fig. 13): on an horizontal line we write the bound. The operator acting on this bound is written **a** and acts twice. Thus two types of states will appear $|l_0\rangle$ and $|l_0'\rangle$. Each time **a** is applied, the bound is ''promoted'' to another state. The prefactor is given by the exponential with the corresponding state of the promoted bound. Then the geometrical diagram can be algebraically written as

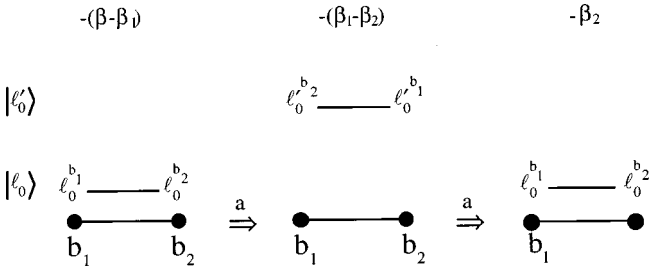

FIG. 13. Geometrical method for computing analytically all types of diagrams. b_1,b_2, represents one tetrahedron. β_i $(i=1,2,...,n)$ is the temperature appearing as an integration variable [see Eq. (B8)].

$$z_0^{N-2}\sum_{(b)}\sum_{|l_0^{b_1}\rangle,|l_0^{b_2}\rangle,|l_0'^{b_1}\rangle,|l_0'^{b_2}\rangle}\langle l_0^{b_1}|\langle l_0^{b_2}|\mathbf{S}_{b_1}\cdot\mathbf{S}_{b_2}|l_0'^{b_1}\rangle|l_0'^{b_2}\rangle$$
$$\times\langle l_0'^{b_1}|\langle l_0'^{b_2}|\mathbf{S}_{b_1}\cdot\mathbf{S}_{b_2}|l_0^{b_1}\rangle|l_0^{b_2}\rangle e^{-(\beta-\beta_1)[E(l_0^{b_1})+E(l_0^{b_2})]}$$
$$\times e^{-(\beta_1-\beta_2)[E(l_0'^{b_1})+E(l_0'^{b_2})]}e^{-\beta_2[E(l_0^{b_1})+E(l_0^{b_2})]}, \qquad \text{(B7)}$$

where (b) is the number of bounds in the lattice. Here this number is easy to compute as there are N sites and each site gives 12 bounds, each of them being counted twice. Thus there are $6N$ bounds and the final result is obtained by integrating with respect to the temperature:

$$6Nz_0^{N-2}\sum_{|l_0^{b_1}\rangle,|l_0^{b_2}\rangle,|l_0'^{b_1}\rangle,|l_0'^{b_2}\rangle}\langle l_0^{b_1}|\langle l_0^{b_2}|\mathbf{S}_{b_1}.\mathbf{S}_{b_2}|l_0'^{b_1}\rangle|l_0'^{b_2}\rangle$$
$$\times\langle l_0'^{b_1}|\langle l_0'^{b_2}|\mathbf{S}_{b_1}.\mathbf{S}_{b_2}|l_0^{b_1}\rangle|l_0^{b_2}\rangle e^{-\beta[E(l_0^{b_1})+E(l_0^{b_2})]}$$
$$\times\int_0^{\beta}d\beta_1 e^{-\beta_1[E(l_0'^{b_1})+E(l_0'^{b_2})-E(l_0^{b_1})-E(l_0^{b_2})]}$$
$$\times\int_0^{\beta_1}d\beta_2 e^{-\beta_2[E(l_0^{b_1})+E(l_0^{b_2})-E(l_0^{b'_1})-E(l_0'^{b_2})]}. \qquad \text{(B8)}$$

With this method, one can evaluate high-order diagrams, as long as the effective model preserves the total ''local'' spin. This procedure can be applied to any kind of model where one can define a perturbative component in the Hamiltonian and where the complete solution of a local part of the Hamiltonian can provide enough information for the global Hamiltonian. The last point is to get rid of the formal anisotropy that we have introduced through the arbitrary choice of numbering of the 4 sites in one tetrahedron. As illustrated in Fig. 8, one sees that between two tetrahedra, there are different types of operators:

$$o^{12}=S_{t_1}^1\cdot S_{t_2}^2;\quad o^{13}=S_{t_1}^1\cdot S_{t_2}^3;\quad o^{14}=S_{t_1}^1\cdot S_{t_2}^4;$$

$$o^{23}=S_{t_1}^2\cdot S_{t_2}^3;\quad o^{24}=S_{t_1}^2\cdot S_{t_2}^4;\quad o^{34}=S_{t_1}^3\cdot S_{t_2}^4,$$

where t_1 and t_2 are two disconnected tetrahedra and the upper indices correspond to the type of site in the unit cell. These operators do not coincide within our notations, so we have to take care of these differences. Nevertheless, as soon as we calculate a physical quantity, this artificial anisotropy disappears as it should, so our approach is coherent.

[1] F. D. M. Haldane, Phys. Rev. Lett. **50**, 1153 (1983).

[2] For reviews, see A. P. Ramirez, Annu. Rev. Mater. Sci. **24**, 453 (1994); P. Schiffer and A. P. Ramirez, Comments Condens. Matter Phys. **18**, 21 (1996); M. J. Harris and M. P. Zinkin, Mod. Phys. Lett. B **10**, 417 (1996).

[3] R. Moessner and J. T. Chalker, Phys. Rev. B **58**, 12 049 (1998); Phys. Rev. Lett. **80**, 2929 (1998).

[4] P. W. Anderson, B. Halperin, and C. M. Varma, Philos. Mag. **25**, 1 (1972).

[5] G. Ferey, R. D. Pape, M. Leblanc, and J. Pannetier, Rev. Chim. Miner. **23**, 474 (1986).

[6] P. Chandra, P. Coleman, and I. Ritchey, J. Phys. I **3**, 591 (1993).

[7] M. J. P. Gingras, C. V. Stager, N. P. Raju, B. D. Gaulin, and J. E. Greedan, Phys. Rev. Lett. **78**, 947 (1997).

[8] M. Shiga, K. Fujisawa, and H. Wada, J. Phys. Soc. Jpn. **62**, 1329 (1993).

[9] M. Mekata, T. Asano, T. Sugino, H. Nakamura, N. Asai, M. Shiga, A. Keren, K. Kojima, G. M. Luke, W. D. Luke, W. D. Wu, Y. J. Uemura, S. Dunsinger, and M. Gingras, J. Magn. Magn. Mater. **140-144**, 1767 (1995).

[10] H. Nakamura, K. Yoshimoto, M. Shiga, M. Nishi, and K. Kakurai, J. Phys.: Condens. Matter **9**, 4701 (1997).

[11] N. P. Raju, E. Gmelin, and R. K. Kremer, Phys. Rev. B **46**, 5405 (1992).

[12] J. N. Reimers, J. E. Greedan, and M. Björgvinsson, Phys. Rev. B **45**, 7295 (1992).

[13] P. Lacorre, J. Phys. C **20**, L775 (1987).

[14] J. S. Gardner, S. R. Dunsiger, B. D. Gaulin, M. J. P. Gingras, J. E. Greedan, R. F. Kiefl, M. D. Lumsden, W. A. MacFarlane, N. P. Raju, J. E. Sonier, I. Swainson, and Z. Tun, Phys. Rev. Lett. **82**, 1012 (1999).

[15] J. E. Greedan, J. N. Reimers, C. V. Stager, and S. L. Penny, Phys. Rev. B **43**, 5682 (1991); J. N. Reimers, J. E. Greedan, C. V. Stager, M. Bjorgvinssen, and M. A. Subramanian, *ibid.* **43**, 5692 (1991).

[16] S. R. Dunsiger, R. F. Kiefl, K. H. Chow, B. D. Gaulin, M. J. P. Gingras, J. E. Greedan, A. Keren, K. Kojima, G. M. Luke, W. A. MacFarlane, N. P. Raju, J. E. Sonier, Y. J. Uemura, and W. D. Wu, Phys. Rev. B **54**, 9019 (1996).

[17] A. S. Wills, N. P. Raju, and J. E. Greedan, Chem. Mater. **11**, 1510 (1999).

[18] E. Greedan, N. P. Raju, A. S. Wills, C. Morin, and S. M. Shaw, Chem. Mater. **10**, 3058 (1998).

[19] N. Fujiwara, H. Yasuoka, and Y. Ueda, Phys. Rev. B **57**, 3539 (1998).

[20] M. J. Harris, M. P. Zinkin, and T. Zeiske, Phys. Rev. B **56**, 11 786 (1997).

[21] M. J. Harris, M. P. Zinkin, Z. Tun, B. M. Wanklyn, and I. P. Swainson, Phys. Rev. Lett. **73**, 189 (1994).

[22] M. Shiga, J. Magn. Magn. Mater. **129**, 17 (1994).

[23] M. Shiga, Physica B **149**, 293 (1988).

[24] R. Ballou, C. Lacroix, and M. D. Nunez-Regueiro, Phys. Rev. Lett. **66**, 1910 (1996).

[25] P. W. Anderson, Phys. Rev. **102**, 1008 (1956).

[26] J. N. Reimers, A. J. Berlinsky, and A.-C. Shi., Phys. Rev. B **43**, 865 (1991).

[27] J. Villain, Z. Phys. B **33**, 31 (1979).

[28] R. Liebmann, *Statistical Mechanics of Periodic Frustrated Ising Systems* (Springer-Verlag, Berlin, 1986).

[29] J. N. Reimers, Phys. Rev. B **45**, 7287 (1992).

[30] S. T. Bramwell, M. J. P. Gingras, and J. N. Reimers, J. Appl. Phys. **75**, 5523 (1994).

[31] R. Sobral and C. Lacroix, Solid State Commun. **103**, 407 (1997).

[32] A. B. Harris, A. J. Berlinsky, and C. Bruder, J. Appl. Phys. **69**, 5200 (1991).

[33] M. Isoda and S. Mori, J. Phys. Soc. Jpn. **67**, 4022 (1998).
[34] B. Canals and C. Lacroix, Phys. Rev. Lett. **80**, 2933 (1998).
[35] MATHEMATICA (Wolfram Research, Inc., Cambridge, 1988).
[36] P. Lecheminant, B. Bernu, C. Lhuillier, L. Pierre, and P. Sindzingre, Phys. Rev. B **56**, 2521 (1997).
[37] Equation (6) in Ref. 34 is wrong. The minus is missing.
[38] B. Canals, M. Mambrini, and F. Mila (unpublished).
[39] J. Villain, R. Bidaux, J. P. Carton, and R. J. Conte, J. Phys. (Paris) **41**, 1263 (1980).
[40] C. L. Henley, Phys. Rev. Lett. **62**, 2056 (1989).
[41] R. Ballou, E. Lelièvre-Berna, and B. Fak, Phys. Rev. Lett. **76**, 2125 (1996).
[42] R. Ballou, E. Lelièvre-Berna, and B. Fak (private communication).
[43] K. Terao, J. Phys. Soc. Jpn. **65**, 1413 (1996).
[44] D. Garanin and B. Canals, Phys. Rev. B **59**, 443 (1999).